ADVANCED OPTICAL MATERIALS
www.advopticalmat.de

Large-Scale Multifunctional Carbon Nanotube Thin Film as Effective Mid-Infrared Radiation Modulator with Long-Term Stability

*Yue Sun, Huicong Chang, Jun Hu, Yangyang Wang, Yudong Weng, Ce Zhang, Shuai Niu, Longfei Cao, Zhao Chen, Nan Guo, Junku Liu, Jiawei Chi, Guohua Li, and Lin Xiao**

Mid-infrared tunable materials have attracted increasing attention for thermal radiation management in various applications ranging from infrared camouflage to radiative thermoregulation. Functional films based on graphene and carbon nanotubes by electrical gating are promising candidates because of their ultrawide spectral range from visible to terahertz and structural flexibility. However, challenges in practical applications remain, such as short cycle life, rapid performance degradation, and difficulties in the synthesis of large-scale electrochromic films. In this paper, a scalable strategy to produce large-scale mid-infrared electrochromic films with long-term stability is demonstrated, in which a sandwich-structured thin film based on multiwalled carbon nanotubes (MWCNTs) is fabricated via a universal roll-to-roll process. By ionic liquid gating, the electrochromic films exhibit tunable thermal emissivity from ≈0.15–0.7 and excellent stability with 96% modulation retention over 3500 cycles. This mid-infrared electromodulation behavior is mainly ascribed to the change in free carrier concentration of few-walled carbon nanotubes in MWCNT films via a reversible ion-induced doping process. The electrochromic films are found to enable effective radiative thermal regulation, dependent on tunable thermal emissivity. Moreover, applications in infrared displays for secret communication and infrared camouflage for varied environmental backgrounds are also demonstrated with 10 × 10 multipixel arrays.

1. Introduction

Controlling thermal radiation from objects has become an attractive method for applications in infrared camouflage,[1–4] thermography,[5] and radiative thermal management.[6–12] Materials with tunable mid-infrared emissivity are the key to flexible radiative heat regulation, and therefore have been intensely investigated, including thermally induced phase transition materials[1,2,13] mechanically driven elastomer materials,[7,14] and electrically stimulated electrochromic materials.[3,4,8–10,15] Recently, graphene-based flexible electrochromic film has been shown to be a new type of active thermal surface capable of efficient and fast electrical-control of thermal radiation in mid-infrared range.[3,4] However, this functional film suffers from quick performance degradation, dropping to half of the initial modulation depth over hundreds of cycles. Meanwhile, the complicated fabrication process by etching the metal foil substrate of graphene could pose a significant challenge to large-scale, low-cost electrochromic applications.

Similar to graphene, single-walled carbon nanotubes (SWCNTs) possess adjustable Fermi levels and electrical conductivity, making them useful candidates as electrochromic materials.[16–20] It has been reported that the visible and near-infrared absorptivity of semiconductor SWCNT films can be efficiently modulated by electrochemical doping or electrolyte gating, thereby suppressing interband transitions as the Fermi level changes.[18–21] In addition, Haddon and co-workers found that the changing free carrier excitation of semiconductor SWCNTs results in adsorption modulation in the mid- and far-infrared spectral range.[18] However, little work has been done on the electrochromic characteristics of multiwalled carbon nanotubes (MWCNTs), which are not yet considered ideal electrochromic candidates owing to their metallic electronic properties. In this work, we develop a universal roll-to-roll process to manufacture large-scale mid-infrared electrochromic films based on MWCNTs, which act as the electrochromic layer and electrode at the same time. The functional films exhibit an efficient electrochromic modulation capability with a thermal emissivity in the range of ≈0.15–0.7 by

Y. Sun, Dr. H. Chang, Dr. Y. Wang, Y. Weng, Dr. C. Zhang, Dr. Z. Chen, Dr. N. Guo, Dr. J. Liu, Prof. L. Xiao
Nanophotonics and Optoelectronics Research Center
Qian Xuesen Laboratory of Space Technology
China Academy of Space Technology
Beijing 100094, China
E-mail: xiaolin@qxslab.cn

Dr. J. Hu
Inertial Sensors Research Center
Beijing Institute of Control Engineering
Beijing 100094, China

S. Niu, L. Cao, J. Chi, Prof. G. Li
Department of Materials Science and Engineering
School of Mechanical Electronic and Information Engineering
China University of Mining and Technology
Beijing 100083, China

The ORCID identification number(s) for the author(s) of this article can be found under https://doi.org/10.1002/adom.202001216.

DOI: 10.1002/adom.202001216

ionic liquid (IL) gating and a cycling stability that is over graphene-based electrochromic films, reaching about 3500 cycles with 96% modulation retention. Both anionic intercalation into the MWCNTs and ionic adsorption on the MWCNTs could contribute to a noticeable increase in the hole or electron concentration of few-walled carbon nanotubes in the MWCNT networks, which leads to increased electrical conductivity and decreased emissivity in the mid-infrared spectral range. Finally, we demonstrate the applications of these electrochromic films as an adjustable radiative cooling film for temperature regulation, and as a fundamental building block in infrared displays or camouflage. More importantly, this MWCNT film has been commercialized on a meter-scale, which is much cheaper than SWCNT and graphene film. This may greatly advance the practical application of electrochromic devices based on MWCNTs.

2. Results and Discussion

2.1. Fabrication and Modulation Performances of MWCNT-Based Functional Films

A sandwich-structured mid-infrared radiation modulator was fabricated using a scalable roll-to-roll process (**Figure 1**a), using carbon nanotube films as electrochromic materials as well as electrodes, mid-infrared transparent porous membranes (Celgard2325, 25 µm thickness, polypropylene/polyethylene/polypropylene) as the spacer, and HMIm[NTf_2] (1-hexyl-3-methylimidazolium bis(trifluoromethylsulfonyl)imide) as the ionic liquid. The carbon nanotubes, composed of MWCNTs with a diameter between 4 and 15 nm (Figure S1, Supporting Information), were synthesized by a floating catalyst chemical vapor deposition (CVD) method, then rolled into a uniform film and further densified by ethanol–water solution. The thickness of the resulting MWCNT films was ≈10 µm and the surface density was about 0.47 mg cm^{-2} in the latter part of this study without otherwise specified specification. Two layers of the MWCNT films were attached to the Celgard membrane by surface adhesion of the ionic liquid via the roll-to-roll process. It is worth noting that an appropriate amount of ionic liquid, roughly as thick as the Celgard membrane per unit area, was sprayed onto the Celgard membrane to prevent excessive ionic liquid from penetrating and contaminating the outer surface of the MWCNT films.

As shown in Figure 1b, the mid-infrared radiation modulator based on MWCNT films can be gated by nonvolatile ionic liquid through electrochemical doping. By electrical modulation, the electrochromism of MWCNT films could be attributed to two types of processes: 1) adsorption/desorption of cations or anions on the surface of the MWCNTs and 2) intercalation/deintercalation of anions into the graphite layers of the MWCNTs. This will be discussed in detail in Section 2.2. A large flexible electrochromic thin film with a size of 28 × 14 cm^2 was fabricated as shown in Figure 1c. This large-area and infrared radiation-modulated MWCNT device can be widely used in thermal management applications. By applying an electrical voltage to the two MWCNT electrodes, this functional film can act as an infrared cloak for human stealth. As shown in Figure 1d, when a voltage of –1.7 V was applied to the top layer of the MWCNT film, the waist of the human body exhibited a state of high emissivity. When the voltage was 4 V, the human body could blend into the surrounding environment with low emissivity. In addition, even for large-area devices with 45 × 7.5 cm^2, the voltage drop on the

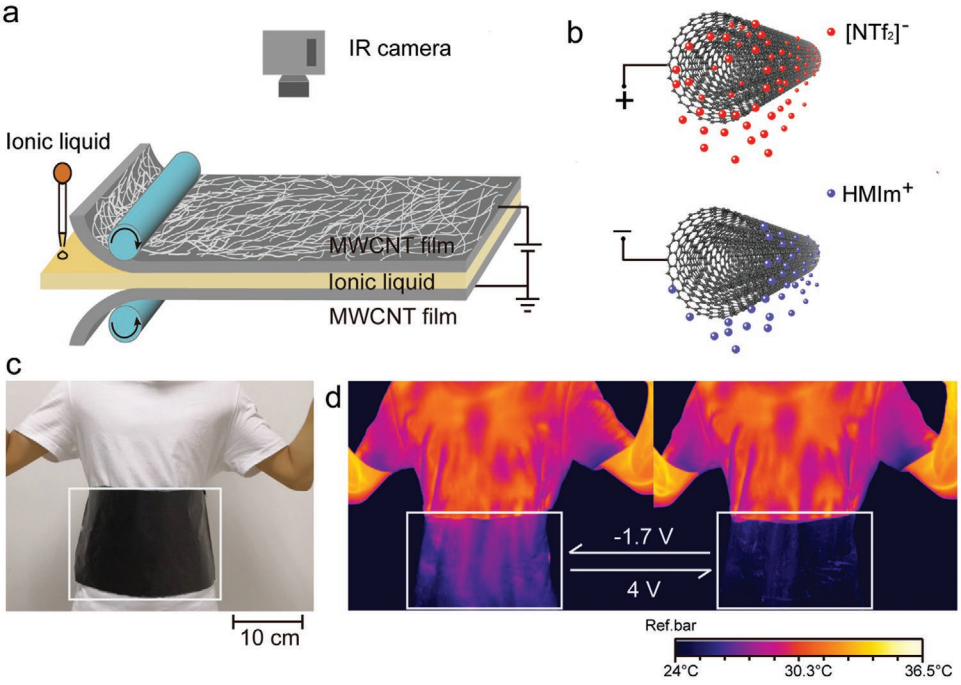

Figure 1. Fabrication and thermal camouflage of the MWCNT-based mid-infrared modulator. a,b) Schematic of the roll-to-roll process to fabricate a sandwich-structured MWCNT/IL-Celgard/MWCNT film. c) Optical image of a flexible large-area functional film adhered to human waist. d) Thermal images of the as-fabricated film with negative (–1.7 V) and positive voltages (4 V), respectively.

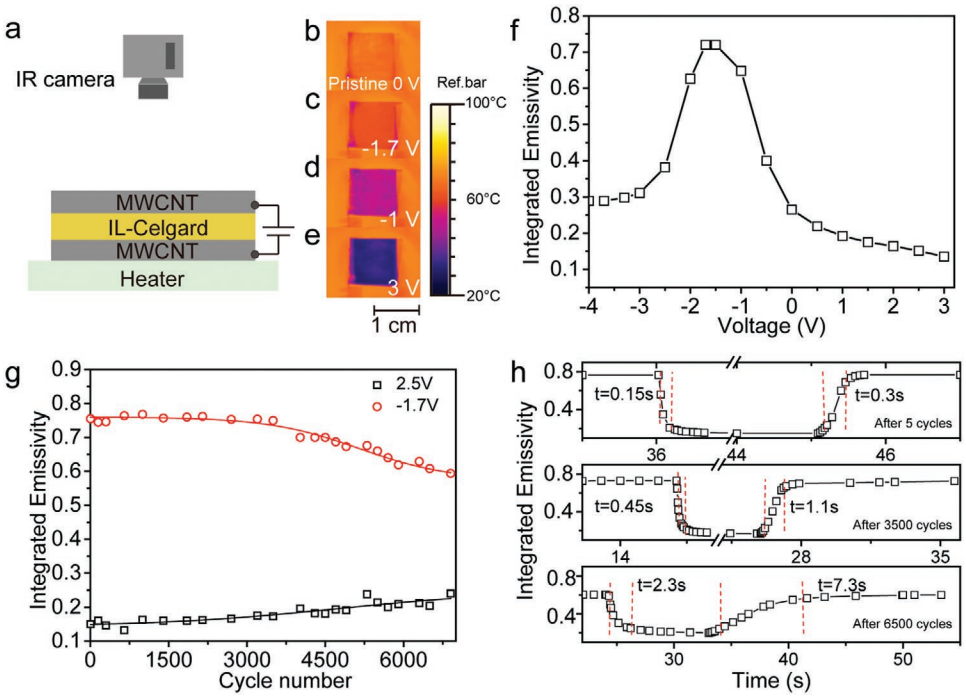

Figure 2. The modulation performance of MWCNT-based functional films with 10 µm thickness. a) Schematic of the experimental setup. b–e) Thermal images of the top MWCNT layer in pristine state and biased at –1.7, –1, and 3 V, respectively. f) The voltage-dependent emissivity of the top MWCNT layer biased from –4 V to 3 V. g) Long-term stability test for a cycle period of 30 s at 50 °C. h) Transient emissivity response, recorded by the thermal camera, to electrical pulse input (20 s at –1.7 V and 10 s at 2.5 V) after 5, 3500, and 6500 cycles, respectively.

surface of the MWCNT film in the length direction was less than 0.05 V, and there was almost no voltage drop in the width direction (Figure S2, Supporting Information). Such a small voltage drop was ascribed to the high conductivity of the MWCNT film with a sheet resistance of 1 Ω sq^{-1}, resulting in uniform modulation performance even for large-area devices.

According to the Stefan–Boltzmann law, the radiant energy per unit area is determined by the temperature of the object and its surface emissivity. As shown in the experimental setup in **Figure 2**a, a thermal camera (spectral range: 7.5–13 µm, PI640, Optris Inc.) was used to measure the emissivity–voltage relationship of a functional film with a size of 1×1 cm^2 and 10 µm thickness, which was placed on a 70 °C heating plate. The total mass of both the top and bottom layer MWCNTs was only about 0.94 mg. As shown in Figure 2b–e, when the voltage of the top MWCNT layer varied from –1.7 to 3 V, the IR temperature of the film decreased significantly from ≈60 to 33 °C. The electrochromic modulation of this film in the voltage range –4 to 3 V was investigated by considering the electrochemical window of the ionic liquid that we used.[22] Owing to the symmetry of the structure, both MWCNT layers of the film exhibited the same emissivity modulation characteristics (Figure S3, Supporting Information). The integrated emissivity can be determined by a commonly used procedure, as described in our previous work.[1,4] Briefly, the integrated emissivity of the target was determined by modifying the emissivity in the thermal camera until the infrared temperature was equal to that measured by a thermocouple. For the top-layer MWCNT film, the integrated emissivity could be adjusted from ≈0.7 at –1.7 V to 0.15 at 3 V (Figure 2f). Moreover, the emissivity modulation performance was independent of film thickness between 10 and 20 µm, as shown in Figure S4 in the Supporting Information. The average power consumption to maintain the corresponding states were 0.94 and 4.85 W m^{-2}, respectively. Such a high modulation depth of the MWCNT film can suppress thermal radiation by 6.7 dB, making this MWCNT-based functional film a promising material for adaptive infrared camouflage. With respect to power consumption, the MWCNT electrochromic device could maintain a relatively low emissivity in an open circuit. As shown in Figure S5 in the Supporting Information, the emissivity of the full charged device at 2.5 V increased from 0.17 to 0.28 during the initial 4 h of the open circuit. The fraction of $\Delta\varepsilon$ retained decreased to 80%. Until the 17th hour, the emissivity remained stable, retaining ≈80% of the emissivity. The fraction of $\Delta\varepsilon$ retained is defined as $\frac{\varepsilon_{max}-\varepsilon_t}{\varepsilon_{max}-\varepsilon_{min}} \times 100\%$,[23] where ε_{max} is the emissivity of the charge-neutral state at –1.7 V, ε_{min} is the emissivity of the holes-doped state at 2.5 V, and ε_t is the real-time emissivity of the open-circuit device. This allowed for a lower total power consumption compared to that required for a continuous power input to maintain a stable state.

The response time and long-term stability are also critical parameters for electrochromic films in future applications. The cycling stability of the functional films was observed using a continuous square wave voltage input of 2.5 and –1.7 V for the low and high emissivity states, respectively, for a period of 30 s at 50 °C. As shown in Figure S6 in the Supporting Information, the current decayed exponentially as a function of time under the square wave voltage, indicating capacitive charging. Integrating the current yielded a total injected charge of 0.05 C

for a sample of 1×1 cm^2 and 10 µm thickness from the highest emissivity (neutral state) to the lowest emissivity (holes-doped state). The MWCNT-based electrochromic films exhibited much better stability than graphene-based functional films. As shown in Figure 2g, the MWCNT-based functional film maintained 96% of its initial emissivity modulation depth over ≈3500 cycles, which was nearly eight times longer than that of graphene-based films reported in our previous work.[4] To measure the response time of the device, an infrared camera (frame rate 32 Hz) was used to record the transient emissivity of the film under the square wave voltage input. As Figure 2h shows, the low-high and high-low durations (10% and 90% of the step height) were about 0.3 and 0.15 s at the 5th cycle and increased to 7.3 and 2.3 s after 6500 cycles. The degradation of the response time can be ascribed to the generation of byproducts at the MWCNT/IL interface, which could lead to slower ion transport through the interphase as well as into and out of the electrode.[24] However, when the device was fully charged with enough time in every cycle, the ions could be adequately intercalated/deintercalated into the MWCNTs and adsorbed/desorbed on the MWCNTs, and the emissivity of the functional film remained in the initial state even over 10 000 cycles, as shown in Figure S7 in the Supporting Information.

In addition, the response times of devices with different thicknesses and areas are shown in Table S1 in the Supporting Information. The devices were a little slower when the film thickness increased from 10 to 20 µm owing to a longer ion diffusion distance in the MWCNT film. The response time was a little change with increasing film areas from 1×1 to 2×2 cm^2. The comprehensive performance of our MWCNT electrochromic device (such as modulation depth, response speed, lifetime, and low cost) was superior to that of other reported mid-IR radiation devices as shown in Table S2 in the Supporting Information.

2.2. Characteristics of MWCNT-Based Films during Electrical Gating

The electrochromic phenomenon can be attributed to two types of processes: adsorption/desorption of cations or anions on the surface of MWCNTs and intercalation/deintercalation of anions into the graphite layers of MWCNTs, as demonstrated by in situ X-ray diffraction (XRD) and Raman spectrum measurements. **Figure 3**a shows the XRD results of the top layer MWCNT films at various voltages. The (002) graphite peak of the pristine MWCNT film was observed at $2\theta = 25.9°$. During the first cycle, the (002) peak was nearly unchanged when the applied voltages were varied from −3 to 0 V. However, as the voltage increased from 0 to 3 V, the (002) peak dramatically downshifted and gradually vanished. The changes in the XRD spectra can be ascribed to the limited expansion of the tubular graphene structure of the MWCNTs due to anion intercalation into the MWCNTs. An amorphous structure inside the fully charged MWCNTs was formed.[25,26] The position of the (002) peak could not completely recover to its initial state at −3 V and its intensity gradually weakened in subsequent cycles, which

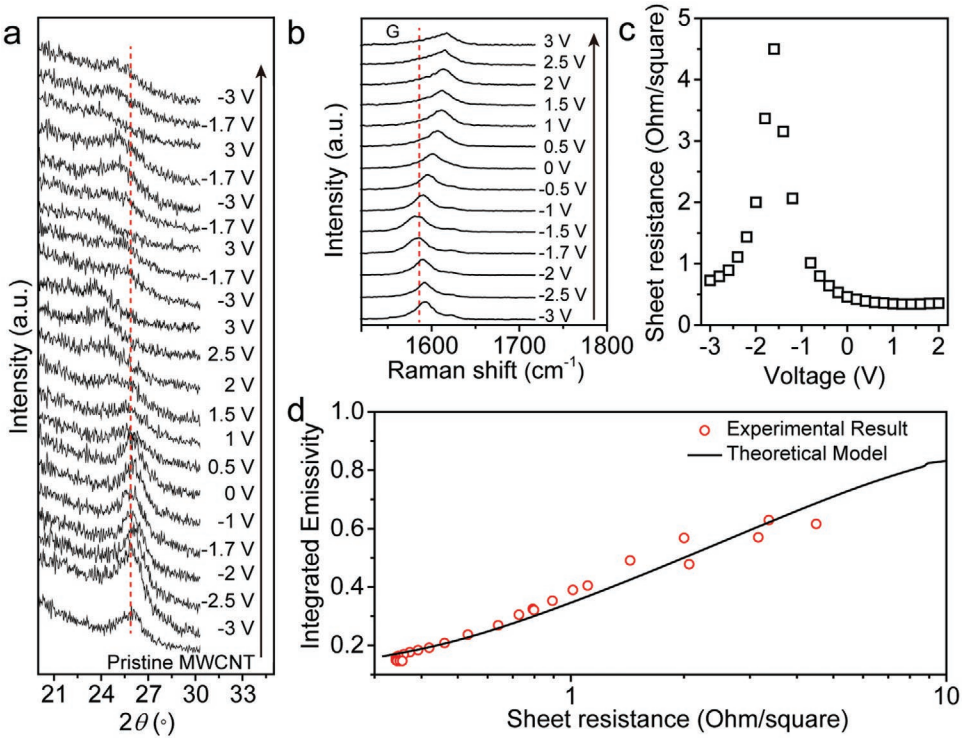

Figure 3. Characteristics of the top layer MWCNT film during the electrochromic process. a) In situ XRD spectra with different applied voltages for the MWCNTs/IL-Celgard/MWCNTs sample. The red line corresponds to (002) graphite peak of pristine MWCNT film. b) In situ Raman spectra of the device at different applied voltages. The red line corresponds to G-peak at −1.7 V. c) Sheet resistance of MWCNT film as a function of gate voltage for the device. d) Dependence of emissivity of the device on its sheet resistance. The red dots and black line represent the experimental results and theoretical calculation based on the effective medium theory and Drude model, respectively.

might be the result of irreversible structural damage during the intercalation/deintercalation processes.

As the G-band depends strongly on the charge carrier density of graphite,[27,28] in situ Raman measurements were conducted to further understand the electrochromic mechanism of the functional film. After several initial cycles, the G-peak showed a blueshift in comparison with that at ≈–1.7 V (≈1584 cm^{-1}), as shown in Figure 3b, which suggests that the carrier concentration of the MWCNT film reaches a minimum value at –1.7 V. The minimum conductivity at negative voltage may be related to the initial p-type characteristics of MWCNTs due to oxygen impurities in the atmosphere.[29] As positive voltages are applied to the top layer MWCNT film, anions accumulate to form a double-layer electric capacitor on the MWCNTs, and a portion of them further intercalate into MWCNTs as indicated by the XRD spectra in Figure 3a. This is also confirmed by the cyclic voltammetry measurement in Figure S8 in the Supporting Information, which indicates physicochemical processes including adsorption/desorption and intercalation/deintercalation of the ions.[25] The adsorption and intercalation of anions result in further hole doping of MWCNTs and increase the conductivity of the functional film. However, as the voltages decreased from 0 to –3 V, the accumulated cations gradually neutralize the electric field caused by the initial oxygen adsorbates on MWNCTs, resulting in an electron doping state with increasing conductivity when the voltage is lower than –1.7 V. Combining the in situ XRD and Raman results given above, it shows that both anionic intercalation and adsorption effects occur simultaneously in the positive voltage range, while cationic adsorption occurs mainly in the negative voltage range. The microscopic differences are also reflected in the asymmetric behavior of the film's conductivity with different gate voltages (Figure 3c). The sheet resistance of the film tends to have a specific value in the negative voltage range owing to the hole doping resulting from saturation adsorption of the cations on the surface of MWCNTs, while it increases due to electron doping resulting from the additional anionic intercalation process at positive voltages.

The effective electrical modulation of the MWCNT film's conductivity could be attributed to the ionic doping of the few-walled CNTs in the film. As shown in Figure S1 in the Supporting Information, the diameters of MWCNTs were widely distributed and most of these tubes were less than 10 nm in diameter, even with double walls, which have low density of states around the Fermi level,[30] and thereby their conductivity can be significantly modulated through ionic doping like single walled CNTs.[31,32] The ions adsorption and anions intercalation resulted in the p or n doping of the few-walled CNTs within the MWCNT film we used, changing the film's conductivity and further the emissivity. In order to further validate our explanation, we measured the electrical property of super-aligned MWCNTs[33] gated by ionic liquid. As shown in Figure S9 in the Supporting Information, the conductivity of super-aligned MWCNT film was hard to modulate by ionic doping, resulting in a small change of thermal emissivity from 0.69 to 0.8. Compared with the tangled MWCNT film with few-walled CNTs, super-aligned MWCNTs have a uniform diameter distribution of about 15 nm,[33] whose carrier concentrations are high and hard to modulate by ionic doping.

To explain the sheet resistance dependence of the thermal emissivity, the effective medium theory was used to describe the dielectric function of the MWCNT film, which is regarded as a mixture of air, ions liquid, and MWCNTs (see details in Section 12 of the Supporting Information). The dielectric function of the constituent MWCNTs was dominated by intraband effects. Therefore, the Drude model was used to calculate the dielectric parameters of the doped MWCNTs.[34] Considering the relationship between gate voltage and the integrated emissivity of the MWCNT film, the dependence of the measured emissivity on the sheet resistance is given in Figure 3d. The theoretical model fits well with our experimental results (see details in Section 12 of the Supporting Information).

2.3. Tunable Radiative Thermoregulation Demonstration

The good performance of MWCNT-based mid-infrared films with considerable modulation depth, fast response, and long-term stability makes them a promising building block for thermal management. Tunable radiative thermoregulation has been in increasing demand to satisfy more flexible temperature control requirements for humans, buildings, and spacecraft.[6,7,9,35–40] We constructed an experimental setup (**Figure 4**a) to demonstrate that this functional film can act as a mid-infrared adjustable surface for a heater to realize radiative temperature regulation (see the Experimental Section for details). The temperature of the heater is closely related to the integrated emissivity of the top layer MWCNT film, which determines the radiation heat transfer to the environment. When the integrated emissivity of the functional film's outer layer was set to 0.7 at –1.7 V, it worked in a cooling state at a temperature of $T_{-1.7V}^{\varepsilon=0.7}$. When the integrated emissivity was set to ≈0.2 at 2.5 V, the heater temperature increased in a heating state at $T_{2.5V}^{\varepsilon=0.2}$. The temperature variation was defined as $\Delta T = T_{2.5V}^{\varepsilon=0.2} - T_{-1.7V}^{\varepsilon=0.7}$. The input power of the heater did not change throughout the experiment. The input power of the heater was 0.658 W and the ambient temperature was fixed at 15 °C. As shown in Figure 4b, when the outer layer MWCNT film was set at 2.5 V, the heating state temperature $T_{2.5V}^{\varepsilon=0.2}$ was 63.1 °C. Inversely, the cooling state temperature $T_{-1.7V}^{\varepsilon=0.7}$ with a high emissivity decreased to 55.1 °C. Compared with this temperature variation of 8 °C in vacuum, the electrochromic tunable temperature variation decreased to 4.7 °C in air due to the air convection (Figure S10, Supporting Information).

To theoretically predict the temperature tunability of the functional films, the temperature variation was calculated at different ambient and heater temperatures. The details of the theoretical model are shown in Section 14 of the Supporting Information. When the ambient temperature was kept at 15 °C, the temperature variation by emissivity modulation dramatically increased with the heater temperature $T_{-1.7V}^{\varepsilon=0.7}$ (Figure 4c), proving the possibility of ≈9 °C at $T_{-1.7V}^{\varepsilon=0.7} = 65$ °C experimentally. The temperature variation is inversely proportional to the ambient temperature with a fixed heater temperature as shown in Figure 4d.

2.4. Infrared Display and Adaptive Thermal Camouflage Demonstrations

The MWCNT-based electrochromic films can also find various applications in infrared displays and in adaptive thermal

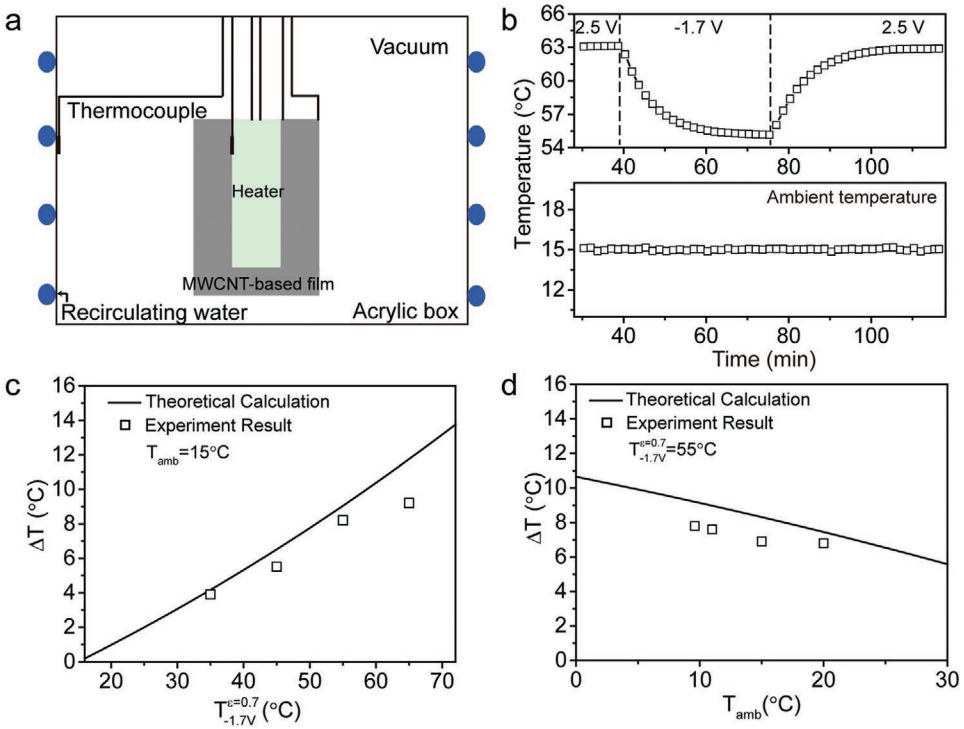

Figure 4. Radiative thermoregulation of MWCNTs/IL-Celgard/MWCNTs device in vacuum. a) Schematic thermal measurement setup of the device. b) Real-time thermal measurements of the device with −1.7 V and 2.5 V applied at ambient temperature of ≈15 °C. c) Dependence of tunable ΔT on the heater temperature $T_{-1.7V}^{\varepsilon=0.7}$ (the black line is the theoretical result and the black squares are experimental results). d) Dependence of temperature variation of the heater on ambient temperature (the black line is the theoretical calculation and the black squares are experimental results).

camouflage. As shown in **Figure 5**a, a device was fabricated on a printed circuit board with 10 × 10 arrays, which can drive each MWCNT element individually. All the elements in the arrays share a large MWCNT film as the common ground counter electrode (Figure 5b). A silicone rubber heater was pasted on the back of the device to simulate a hot source that needed to be hidden. By controlling the voltage of each element in the arrays from −3 to 1.7 V, the integrated emissivity of the corresponding region of the top-layer MWCNT film could be adjusted from 0.15 to 0.7. Thermal imaging (Figure 5c–f) shows that the device can be modulated to display different letters (Movie S1, Supporting Information), where the integrated emissivity of the letters was set to 0.7 and the rest at 0.15. The clear pixel boundaries between letters and their surrounding regions suggested that each element can be well modulated without its electric field interacting with the others.

This behavior will also facilitate adaptive infrared camouflage in complex environments. The total thermal radiance M_{total} detected by an infrared camera from an object can be expressed as[1]

$$M_{\text{total}} \approx \varepsilon_{\text{obj}}\left(S_{\text{obj}} - S_{\text{amb}}\right) \tag{1}$$

where ε_{obj} is the integrated emissivity of the object and S_{obj} and S_{amb} are the integrated thermal radiance of a blackbody at object (T_{obj}) and ambient (T_{amb}) temperature, respectively, in the infrared camera's spectral range. Therefore, objects with the same thermal radiance (M_{total}) cannot be distinguished by an infrared camera, demonstrating infrared stealth. Here we simulated a background environment with different temperature regions to demonstrate the infrared stealth capability of the functional films. As shown in Figure 5g, an MWCNT-based electrochromic device at 70 °C was placed in front of three colors of acrylic plates (integrated emissivity 0.95) as backgrounds, which were heated to 33, 40, and 60 °C with white, yellow, and black colors, respectively. By programming the thermal emissivity of the elements, the functional device could blend naturally into the surrounding background with the infrared camera (Figure 5h). The integrated emissivity was adjusted to ≈0.15, 0.26, and 0.7 for the white, yellow, and black backgrounds, with the voltages of −3, 0.5, and 1.7 V, respectively. And the corresponding calculated values of emissivity are 0.18, 0.31, and 0.72 according to Equation (1), respectively. The theoretical and experimental deviations are mainly due to the temperature inhomogeneity of the backgrounds shown in Figure 5i. Figure 5j,k shows the quantitative infrared temperature distribution of the device and the backgrounds recorded by a thermal camera, where except for the edge regions, the MWCNT-based arrays match very well with the background against infrared surveillance.

3. Conclusion

In conclusion, we have successfully fabricated large-area mid-infrared modulators based on MWCNT films via a scalable roll-to-roll manufacturing process. Ionic liquid doping into the MWCNTs leads to a considerable change in the integrated

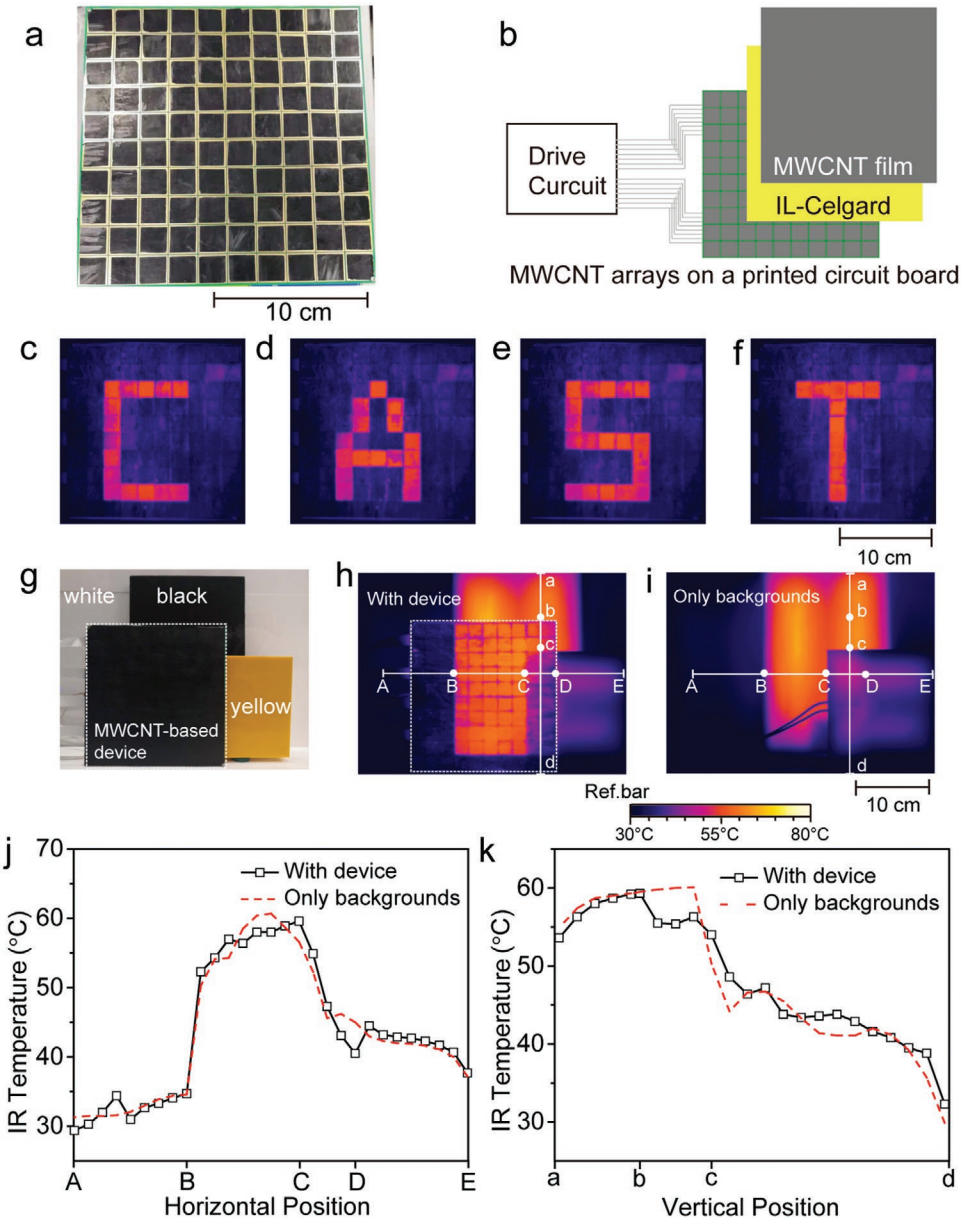

Figure 5. Infrared display and adaptive thermal camouflage demonstrations for an MWCNT-based multipixel device. a) Optical picture of a multipixel device with 10 × 10 MWCNT arrays on a printed circuit board. b) Schematic diagram of the device, composed of bottom MWCNT arrays, Celgard membrane with ionic liquid, a common ground counter MWCNT film, and a drive circuit for the printed circuit board. c–f) Thermal images of the device at ≈65 °C to display different letters "CAST" by programming the emissivity of the arrays. g,h) Visual and thermal infrared images of the MWCNT-based multipixel device at 70 °C in front of three colors of acrylic plates, white 33 °C, yellow 40 °C, and black 60 °C. i) Thermal infrared image of the backgrounds. j,k) Horizontal and vertical IR temperature distribution of the thermal images in (h,i).

emissivity from ≈0.7 to 0.15 within a second. The device exhibits long-term cyclic stability with 96% modulation retention over 3500 cycles. The mid-infrared modulator based on MWCNTs shows tunable radiative temperature regulation capabilities in both vacuum and atmospheric conductions, which makes it attractive for the fields of energy-saving and thermoregulation. Moreover, the superior performance of the MWCNT-based mid-infrared modulator with a large modulation depth, fast speed, and high stability promises potential applications in infrared security communication and adaptive thermal camouflage.

4. Experimental Section

Physical Characterization: The thickness of the MWCNT films was measured by a step profiler (P-7, KLA-Tencor Inc.) on a glass substrate. transmission electron microscope (TEM) imaging was performed using a TEM (JEM-2100F, JEOL Inc.). In situ XRD patterns were measured using an X-ray diffractometer (Smartlab Inc.) and Raman spectra was measured with a micro-Raman spectrometer (JY HR-800, Horiba Inc.) at a laser wavelength of 514 nm. The voltage bias was applied by a Keithley 2612B source meter in the measurements.

MWCNT Film Synthesis and Device Fabrication: The MWCNT films were synthesized using a floating catalyst CVD method. Under a reducing

H_2 and Ar environment, a mixed liquid of ethanol, thiophene, and dicyclopentadienyl iron was injected into the furnace at 1200–1300 °C. The formed continuous and fluffy MWCNTs were collected on a roller and further moved to the platform to be compacted and densified by a methanol–water solution.[41] The device fabrication process was as follows: the compacted MWCNT film with a thickness of 10 µm was cut into pieces with suitable size by a blade. Then, enough ions liquid was dropped onto the surface to fully wet one MWCNT film, which was defined as the bottom layer MWCNT film. A larger area Celgard membrane was then covered with the bottom layer of the MWCNT film. It is important to ensure the wettability of the ionic liquid on the surface of MWCNT film and the Celgard membrane. Finally, the top layer of the MWCNT film covered the Celgard membrane through a homemade roll-to-roll setup to ensure that there are no air bubbles between the layers. Note that a small amount of ionic liquid was sprayed on the upper surface of the Celgard membrane to ensure its adhesion with the top-layer MWCNT film. The electrodes were formed by two wires attached to the two MWCNT films by silver conductive adhesive.

Integrated Emissivity and Thermochromic Response Measurement: The integrated emissivity was measured by a thermal camera (PI640, Optris Inc. spectral range from 7.5 to 13 µm, frame rate 32 Hz) following a standard procedure in industry. The temperature of the MWCNT-based functional films was measured by a thermocouple (Pt100 temperature sensor) and controlled using a temperature controller (Model 332 temperature controller, Lake Shore Cryotronics Inc.). The integrated emissivity was obtained by adjusting the emissivity in the thermal camera until the infrared temperature was the same as that of the thermocouple. The thermochromic time response was obtained by analyzing each frame of a video recorded by the thermal camera at a frame rate of 32 Hz.

Radiative Thermoregulation Demonstration: The temperature of the heater was measured at a vacuum ambient temperature. The heater was assembled using a ceramic electric heater (2 cm × 2.3 cm), a thin copper wire and 3M tape, and then surrounded by the MWCNT-based device. A thermocouple (Pt100 temperature sensor) was embedded in the copper layer to monitor heater temperature in real time. The entire device was enclosed in an IR-opaque, visibly transparent acrylic chamber with recycled water to control the chamber air temperature, which was measured by the same thermocouple located above the center of the heater. When a voltage of –1.7 or 2.5 V was applied to the device, the temperature of the heater changed to the corresponding values due to the emissivity change of the top layer MWCNT film. It is worth noting that Joule heating of the MWCNT-based device contributes little when reaching thermal equilibrium in the measurement.

Fabrication of the MWCNT-Based Multipixel Device, Infrared Display and Adaptive Thermal Camouflage Demonstrations: The MWCNT-based multipixel device consisted of bottom MWCNT arrays, a Celgard membrane with ionic liquid, a common counter MWCNT electrode, and a drive circuit for the printed circuit board. A large-area MWCNT film was cut into 2 × 2 cm^2 pieces using a laser. The small pieces were transferred to a printed circuit board with 100 independently controllable channels to form 10 × 10 arrays. Then, the arrays were successively covered by a Celgard membrane with an ionic liquid and a 20 × 20 cm^2 MWCNT film. The top MWCNT film was grounded and the bottom MWCNT elements were electrically controlled through a drive circuit. Silicone rubber heaters were pasted on the back of the multipixel device and acrylic plates for temperature control. Three colors of acrylic plates were employed to simulate backgrounds at different temperatures. Thermal images and videos were recorded using a thermal camera. By programming the voltages applied to the elements, the multipixel device can display the designed infrared letters or structures in the thermal camera.

Supporting Information

Supporting Information is available from the Wiley Online Library or from the author.

Acknowledgements

Y.S. and H.C. contributed equally to this work. The authors gratefully acknowledge the helpful discussions from Dr. Sai Chen at Tsinghua University. This research was supported by the National Natural Science Foundation of China (Nos. 21905301, 11704406, and 21805304).

Conflict of Interest

The authors declare no conflict of interest.

Keywords

camouflage, electrochemical doping, mid-infrared modulators, multiwalled carbon nanotubes, radiative thermoregulation

Received: July 19, 2020
Revised: October 27, 2020
Published online: November 26, 2020

[1] L. Xiao, H. Ma, J. Liu, W. Zhao, Y. Jia, Q. Zhao, K. Liu, Y. Wu, Y. Wei, S. Fan, K. Jiang, *Nano Lett.* **2015**, *15*, 8365.
[2] Y. Qu, Q. Li, L. Cai, M. Pan, P. Ghosh, K. Du, M. Qiu, *Light: Sci. Appl.* **2018**, *7*, 26.
[3] O. Salihoglu, H. B. Uzlu, O. Yakar, S. Aas, O. Balci, N. Kakenov, S. Balci, S. Olcum, S. Süzer, C. Kocabas, *Nano Lett.* **2018**, *18*, 4541.
[4] Y. Sun, Y. Wang, C. Zhang, S. Chen, H. Chang, N. Guo, J. Liu, Y. Jia, L. Wang, Y. Weng, W. Zhao, K. Jiang, L. Xiao, *ACS Appl. Mater. Interfaces* **2019**, *11*, 13538.
[5] A. Tittl, A.-K. U. Michel, M. Schäferling, X. Yin, B. Gholipour, L. Cui, M. Wuttig, T. Taubner, F. Neubrech, H. Giessen, *Adv. Mater.* **2015**, *27*, 4597.
[6] P.-C. Hsu, C. Liu, A. Y. Song, Z. Zhang, Y. Peng, J. Xie, K. Liu, C.-L. Wu, P. B. Catrysse, L. Cai, S. Zhai, A. Majumdar, S. Fan, Y. Cui, *Sci. Adv.* **2017**, *3*, e1700895.
[7] E. M. Leung, M. C. Escobar, G. T. Stiubianu, S. R. Jim, A. L. Vyatskikh, Z. Feng, N. Garner, P. Patel, K. L. Naughton, M. Follador, E. Karshalev, M. D. Trexler, A. A. Gorodetsky, *Nat. Commun.* **2019**, *10*, 1947.
[8] S. Chen, Z. Wang, H. Ren, Y. Chen, W. Yan, C. Wang, B. Li, J. Jiang, C. Zou, *Sci. Adv.* **2019**, *5*, eaav6815.
[9] J. Mandal, S. Du, M. Dontigny, K. Zaghib, N. Yu, Y. Yang, *Adv. Funct. Mater.* **2018**, *28*, 1802180.
[10] P. Chandrasekhar, B. J. Zay, G. C. Birur, S. Rawal, E. A. Pierson, L. Kauder, T. Swanson, *Adv. Funct. Mater.* **2002**, *12*, 95.
[11] P. Chandrasekhar, B. J. Zay, D. Lawrence, E. Caldwell, R. Sheth, R. Stephan, J. Cornwell, *J. Appl. Polym. Sci.* **2014**, *131*, 40850.
[12] J. G. Metts, J. A. Nabity, D. M. Klaus, *Adv. Space Res.* **2011**, *47*, 1256.
[13] M. A. Kats, R. Blanchard, S. Zhang, P. Genevet, C. Ko, S. Ramanathan, F. Capasso, *Phys. Rev. X* **2013**, *3*, 041004.
[14] C. Xu, G. T. Stiubianu, A. A. Gorodetsky, *Science* **2018**, *359*, 1495.
[15] K. Sauvet, L. Sauques, A. Rougier, *Sol. Energy Mater. Sol. Cells* **2009**, *93*, 2045.
[16] M. L. Moser, G. Li, M. Chen, E. Bekyarova, M. E. Itkis, R. C. Haddon, *Nano Lett.* **2016**, *16*, 5386.
[17] Y. Gladush, A. A. Mkrtchyan, D. S. Kopylova, A. Ivanenko, B. Nyushkov, S. Kobtsev, A. Kokhanovskiy, A. Khegai, M. Melkumov, M. Burdanova, M. Staniforth, J. Lloyd-Hughes, A. G. Nasibulin, *Nano Lett.* **2019**, *19*, 5836.
[18] F. Wang, M. E. Itkis, E. Bekyarova, R. C. Haddon, *Nat. Photonics* **2013**, *7*, 459.

[19] K. Yanagi, R. Moriya, Y. Yomogida, T. Takenobu, Y. Naitoh, T. Ishida, H. Kataura, K. Matsuda, Y. Maniwa, *Adv. Mater.* **2011**, *23*, 2811.
[20] D. Stekovic, B. Arkook, G. Li, W. Li, E. Bekyarova, M. E. Itkis, *Adv. Mater. Interfaces* **2018**, *5*, 1800861.
[21] K. K. Kim, J. J. Bae, H. K. Park, S. M. Kim, H.-Z. Geng, K. A. Park, H.-J. Shin, S.-M. Yoon, A. Benayad, J.-Y. Choi, Y. H. Lee, *J. Am. Chem. Soc.* **2008**, *130*, 12757.
[22] K. Jayachandran, R. Gupta, M. Sundararajan, S. Gupta, M. Mohapatra, S. K. Mukerjee, *Electrochim. Acta* **2016**, *224*, 269.
[23] F. Berger, T. Higgins, M. Rother, A. Graf, Y. Zakharko, S. Allard, M. Matthiesen, J. Gotthardt, U. Scherf, J. Zaumseil, *ACS Appl. Mater. Interfaces* **2018**, *10*, 11135.
[24] X.-G. Sun, C. Liao, N. Shao, J. R. Bell, B. Guo, H. Luo, D. Jiang, S. Dai, *J. Power Sources* **2013**, *237*, 5.
[25] M. Han, Z. Lv, L. Hou, S. Zhou, H. Cao, H. Chen, Y. Zhou, C. Meng, H. Du, M. Cai, Y. Bian, M.-C. Lin, *J. Power Sources* **2020**, *451*, 227769.
[26] H. Jiao, J. Wang, J. Tu, H. Lei, S. Jiao, *Energy Technol.* **2016**, *4*, 1112.
[27] I. Jeon, B. Yoon, M. He, T. M. Swager, *Adv. Mater.* **2018**, *30*, 1704538.
[28] A. Das, S. Pisana, B. Chakraborty, S. Piscanec, S. K. Saha, U. V. Waghmare, K. S. Novoselov, H. R. Krishnamurthy, A. K. Geim, A. C. Ferrari, A. K. Sood, *Nat. Nanotechnol.* **2008**, *3*, 210.
[29] J. Vavro, M. C. Llaguno, J. E. Fischer, S. Ramesh, R. K. Saini, L. M. Ericson, V. A. Davis, R. H. Hauge, M. Pasquali, R. E. Smalley, *Phys. Rev. Lett.* **2003**, *90*, 065503.
[30] C. J. Christophe, R. Stephan, *Rev. Mod. Phys.* **2007**, *79*, 677.
[31] H. Shimotani, S. Tsuda, H. Yuan, Y. Yomogida, R. Moriya, T. Takenobu, K. Yanagi, Y. Iwasa, *Adv. Funct. Mater.* **2014**, *24*, 3305.
[32] K. Yanagi, R. Okada, Y. Ichinose, Y. Yomogida, F. Katsutani, W. Gao, J. Kono, *Nat. Commun.* **2018**, *9*, 1121.
[33] X. Zhang, K. Jiang, C. Feng, P. Liu, L. Zhang, J. Kong, T. Zhang, Q. Li, S. Fan, *Adv. Mater.* **2006**, *18*, 1505.
[34] M. I. Markovic, A. D. Rakic, *Appl. Optics* **1990**, *29*, 3479.
[35] A. P. Raman, M. A. Anoma, L. Zhu, E. Rephaeli, S. Fan, *Nature* **2014**, *515*, 540.
[36] J. Mandal, Y. Fu, A. Overvig, M. Jia, K. Sun, N. Shi, H. Zhou, X. Xiao, N. Yu, Y. Yang, *Science* **2018**, *362*, 315.
[37] T. Li, Y. Zhai, S. He, W. Gan, Z. Wei, M. Heidarinejad, D. Dalgo, R. Mi, X. Zhao, J. Song, J. Dai, C. Chen, A. Aili, A. Vellore, A. Martini, R. Yang, J. Srebric, X. Yin, L. Hu, *Science* **2019**, *364*, 760.
[38] P.-C. Hsu, A. Y. Song, P. B. Catrysse, C. Liu, Y. Peng, J. Xie, S. Fan, Y. Cui, *Science* **2016**, *353*, 1019.
[39] P.-C. Hsu, X. Liu, C. Liu, X. Xie, H. R. Lee, A. J. Welch, T. Zhao, Y. Cui, *Nano Lett.* **2015**, *15*, 365.
[40] H. Demiryont, D. Moorehead, *Sol. Energy Mater. Sol. Cells* **2009**, *93*, 2075.
[41] T. Ling, T. Chen, Y. Wu, (WuXi YuanWen Graphene Technology Co., Ltd), *CN 109704310A*, **2019**.